Quantum interference near a photonic band edge beyond the weak-field approximation

P. M. Alsing,* D. A. Cardimona,† and D. H. Huang‡
Air Force Research Laboratory, Space Vehicles Directorate, 3550 Aberdeen Ave, SE, Kirtland AFB, Albuquerque, New Mexico 87117-5776, USA
(Received 2 May 2007; published 2 October 2007)

We investigate spontaneous emission and quantum interference effects involving a three-level atom in the vicinity of a photonic band edge beyond the weak-driving-field approximation. We consider two different three-level atoms, each subject to a probe field from the ground state and each embedded within a different photonic crystal (PhC). The first atom has the two excited states separated by a dipole transition in the optical frequency range, with this frequency being close to the surrounding PhC's band edge. The probe field couples the ground state and the highest excited state, and is well outside the PhC band gap. If a coupling field is applied between the two upper levels, electromagnetically induced transparency (EIT) may occur, depending on the position of the band edge. The second atom has the two upper levels each dipole-coupled to the ground state and close enough that the emissions from each can coherently interfere. This atom is embedded within a PhC whose band edge lies near the lower of the two excited states, and a probe field is applied that lies just beyond this band edge. This atom exhibits a quantum interference phenomenon related to EIT called field-induced transparency, again depending on the position of the band edge relative to the lower excited state.

DOI: 10.1103/PhysRevA.76.043802 PACS number(s): 42.70.Qs, 42.50.Fx, 42.50.Gy

I. INTRODUCTION

The study and behavior of multilevel quantum optical systems in the structured reservoirs of photonic band-gap (PBG) materials and photonic crystals (PhCs) has attracted much attention over the last 20 years (see, e.g., [1] and references therein). Early interest concentrated on one-dimensional (1D) PhC structures, while current research and experiments focus on 2D structures, with a strong push towards the fabrication and study of 3D structures.

An early key area of study in PBG materials, which still receives consideration today, is the modification of spontaneous emission by few-level atomic systems in the vicinity of a photonic band edge (PBE). In free space with the linear photon dispersion relation $\omega=kc$, Wigner-Weisskopf theory yields the usual exponential spontaneous emission decay, along with a (Lamb) frequency shift. However, if the density of electromagnetic modes changes rapidly in the vicinity of the atomic transition, the Wigner-Weisskopf (or "pole") approximation [2] is no longer valid. In general, the integrals for the evolution of the atomic system, which involve the solution of the electromagnetic degrees of freedom, must be carried out at some higher level of accuracy beyond the δ-function approximation in order to take into account the non-Markovian nature of the dissipative reservoir.

John and collaborators [3] introduced a simple model of a 3D periodic dielectric material with an exact analytical expression (in terms of a transcendental equation) for the photon dispersion relation ω_k [4]. In the vicinity of the PBE, ω_k can be expanded in a Taylor series to second order in k, without a linear contribution. As reviewed in the Appendix A, this allows one to evaluate integrals directly for the kernel (or Green) functions which govern the non-Markovian evolution of the atomic system. In this model, the presence of the PBE modifies the density of states from that of the usual free space form of $\rho(\omega)\sim\omega^2$ to $\rho(\omega)\sim\Theta(\omega-\omega_{be})/\sqrt{\omega-\omega_{be}}$ where ω_{be} is the band-edge frequency of the PBG.

In a series of papers during the 1990s, John and collaborators [3], as well as other researchers [5], have used the above model to explore the consequences of spontaneous emission and induced atomic decay in the presence of a PBE. The analyses used in the above works follow a Schrödinger picture approach in which the wave function contains components consisting of various atomic states with no photons in the field and a terminal atomic state containing a single photon of arbitrary momentum and direction. Though these analyses go beyond the Wigner-Weisskopf approximation in evaluating the above kernel integrals exactly, they still consider a scenario in which there is at most one quanta in the photon field. The issue of how to progress beyond this single-photon or "weak-field" approximation has been discussed in the literature [1] and only moderately addressed [6].

In this work we present a straightforward density matrix approach which allows us to analyze spontaneous emission and quantum interference effects in the vicinity of a PBE for arbitrary probe and driving field strengths. We develop the density matrix equations by returning to the well-developed theory of spontaneous emission in the Heisenberg picture [7] and rearranging the formulation so that the non-Markovian convolution integrals between the atomic and field degrees of freedom can be dealt with beyond the Wigner-Weisskopf pole approximation for the model of the PBG introduced by John and co-workers and discussed above.

The outline of this paper is as follows: to maintain the flow of analysis and discussion, we relegate to the Appendixes a review of the general interaction between a quantized electric field and a single atomic system consisting of an arbitrary number of levels and the derivations of our density

*Corresponding author. paul.alsing@kirtland.af.mil
†dave.cardimona@kirtland.af.mil
‡danhong.huang@kirtland.af.mil

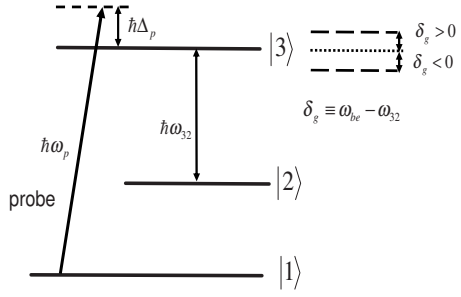

FIG. 1. Energy level diagram for a three-level atom in a V configuration. The optical transition from level 3 to 2 is near the PBE with detuning δ_g, while the transitions from level 2 and 3 to level 1 are far from the PBE.

matrix equations in the vicinity of a PBE. We then use our equations to explore spontaneous emission and quantum interference effects in a three-level atomic system (3LA) near a PBE in three different configurations. In Sec. II we explore the 3LA in which the transition frequency $\omega_{32}=\omega_3-\omega_2$ between the upper two levels (2 and 3) is near the PBE, while the system is interrogated by a probe field from the ground state (level 1) to the upper level (3). It is assumed that the transition frequency ω_{31} is much larger than the PBG so that spontaneous emission between these levels can be assumed to occur as in free space. The same is assumed for the 2-1 transition of frequency ω_{21}. This system was explored by Paspalakis *et al.* [5] in a single-photon Schrödinger wave-function approach discussed above and was found to have a zero in the complex susceptibility (both real and imaginary parts) at a particular probe detuning which depends on the detuning of the PBE from the upper transition $\delta_g \equiv \omega_{be} - \omega_{32}$. Our density matrix formulation of the problem allows us to revisit this configuration beyond the weak-field approximation and to observe power broadening effects. In Sec. III we modify the previous 3LA system by introducing an additional "coupling" field on the 2-3 transition. This allows us to explore the phenomenon of electromagnetically induced transparency (EIT) [8] in the presence of a PBE. In the previous two sections, while the transition frequency ω_{32} is considered detuned from the PBG by a small amount, ω_{32} is considered to be in the optical regime and is thus large with respect to the decay rates γ_2 and γ_3 of levels 2 and 3, respectively, to the ground state (level 1)—i.e., $\omega_{32} \gg \gamma_2, \gamma_3$. In Sec. IV we explore the opposite regime where $\omega_{32} \sim \gamma_2, \gamma_3$. In this situation the dipole radiation from levels 2 and 3 to the ground state can destructively interfere and produce an absorption minimum. This "precursor" phenomenon to EIT was first explored by Cardimona *et al.* [9] and called field-induced transparency (FIT). FIT near a PBE proves to be a nice system to explore since it is a pure interference effect and hence is drastically effected by the detuning of the levels 2 and 3 from the PBE. Finally, in the last section we summarize our results and present our conclusions.

II. THREE-LEVEL ATOM NEAR A PBE

In this section we consider the three-level atom illustrated in Fig. 1 (see [5]). For this system, we consider the transition

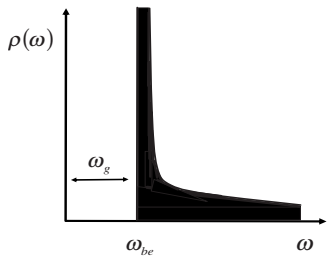

FIG. 2. Density of states for the dispersion relation, Eq. (1), valid near the PBE of frequency ω_{be} and PBG of width ω_g.

frequency between levels 2 and 3 to be near a PBE, while the ground-state level 1 lies far from the PBE, and thus transitions from 2-1 and 3-1 are treated as occurring in free space.

As detailed in the Appendixes, we derive the equations of motion for the density matrix elements $\rho_{ji}(t)$, $j,i \in \{1,2,3\}$, for a three-level atom interacting with an external laser probe field of the form $\vec{E}_L = \vec{e}_L E_L e^{-i\omega_p t} + \text{c.c.}$, taking into account the modification of the spontaneous emission due to the presence of the PBE. For an isotropic model of a PBG the dispersion relation near the PBE takes the form [3]

$$\omega_{\vec{k}} = \omega_{be} + A(|\vec{k}| - |\vec{k}_0|)^2, \quad A = c^2/\omega_g, \tag{1}$$

where ω_{be} is the frequency of the PBE, ω_g is the frequency width of the gap, and $k_0 = |\vec{k}_0| = \omega_g/c$ [10]. The above dispersion relation is valid for $\omega_g \gg c(|\vec{k}| - |\vec{k}_0|)$ and gives rise to a density of states that varies as $\rho(\omega) \sim \Theta(\omega - \omega_{be})/\sqrt{\omega - \omega_{be}}$, (see Fig. 2). For ω_{32} near the PBE, $\delta_g \equiv \omega_{be} - \omega_{32}$ is considered as a slowly varying frequency and the spontaneous emission from level 3 to 2 is modified over that of its free-space value $\rho(\omega) \sim \omega^2$, calculated in the usual Wigner-Weisskopf approximation (see the Appendixes).

A. Exact steady-state solution of density matrix equations

For the three-level atom in Fig. 1 we write the density matrix elements $\rho_{ji}(t)$ in terms of the slowly varying time components $r_{ji}(t)$ as $\rho_{ii}(t) = r_{ii}(t)$, $\rho_{31}(t) = r_{31}(t)e^{-i\omega_p t}$, $\rho_{21}(t) = r_{21}(t)e^{-i(\omega_p - \omega_{32})t} = r_{21}(t)e^{-i(\omega_{21} + \Delta_p)t}$, and $\rho_{32}(t) = r_{32}(t)e^{-i\omega_{32}t}$ and their complex conjugates. Here ω_p is the frequency of the laser probe field and $\Delta_p = \omega_p - \omega_{31}$ is the detuning from the upper level 3. Additionally, levels 2 and 3 are separated by an optical frequency such that $e^{-i\omega_{32}t}$ is considered as a rapidly varying term. In the following, we make a rotating-wave approximation (RWA) and drop terms that oscillate rapidly. We also assume that all the population is initially in the ground state, $r_{11}(t=0) = 1$. The equations of motion for our system are then given by

$$\dot{r}_{22}(t) = -2\gamma_2 r_{22}(t) + [K_{32}(t;0) + K_{32}^*(t;0)] \star r_{33}(t), \tag{2a}$$

$$\dot{r}_{33}(t) = -\{2\gamma_3 + [K_{32}(t;0) + K_{32}^*(t;0)]\star\} r_{33}(t) + i\Omega_p r_{13}(t) - i\Omega_p^* r_{31}(t), \tag{2b}$$

$$\dot{r}_{31}(t) = i\Omega_p [r_{11}(t) - r_{33}(t)] + \{i\Delta_p - [\gamma_3 + K_{32}(t;\Delta_p)\star]\} r_{31}(t), \tag{2c}$$

$$\dot{r}_{21}(t) = (i\Delta_p - \gamma_3)r_{21}(t) - i\Omega_p r_{23}(t), \tag{2d}$$

$$\dot{r}_{32}(t) = i\Omega_p r_{12}(t) - [\gamma_3 + K_{32}(t;0)\star]r_{32}(t), \tag{2e}$$

where $r_{11}+r_{22}+r_{33}=1$. In the above γ_3 and γ_2 are the free-space spontaneous emission rates from level 3 to 1 and level 2 to 1, respectively, and $\Omega_p=(\vec{\mu}_{31}\cdot\vec{e}_L)E_L/\hbar$ is the Rabi frequency between levels 1 and 3. The $\star$ operator denotes a convolution between the non-Markovian kernel function $K_{32}(t;\delta)\equiv K_{3223}(t;\delta)$ (with $\delta\in\{0,\Delta_p\}$) and a density matrix element $r_{ji}(t)$—i.e., $K_{32}(t;\delta)\star r_{ji}(t) = \int dt' K_{32}(t-t';\delta)r_{ji}(t')$—and represents a modification of the spontaneous emission due to the structured vacuum of the PBG. The kernel function $K_{32}(t;\delta)$ is computed in Appendix B and given by Eq. (B7a).

We are interested in the steady-state solution of Eqs. (2a)–(2e), which can be calculated directly by utilizing Laplace transforms (LTs). The above equations have the form $\dot{\vec{r}}(t)=\vec{F}(\vec{r})+\vec{b}$, where $\vec{r}=\{r_{22},r_{33},r_{31},r_{21},r_{32},r_{13},r_{12},r_{23}\}$, $\vec{b}$ is a constant vector of Rabi driving terms, and $\vec{F}(\vec{r})$ contains products of $r_{ji}(t)$ with constant coefficients or convolutions with the kernel function $K(t;\delta)$. Since the LT of a convolution is given by the product of the LTs of the functions in the integrand, the equations of motion takes the linear form $s\tilde{\vec{r}}(s)=A(s)\tilde{\vec{r}}(s)+\vec{b}/s$ with solution $s\tilde{\vec{r}}(s)=[s-A(s)]^{-1}\vec{b}$, where $\tilde{r}_{ji}(s)$ is the LT of $r_{ji}(t)$. The LT $\tilde{K}(s;\delta)$ of the kernel function is given in Eq. (B10). To compute the steady-state solution directly from the solution in LT space we utilize the long-time limit theorem LT [11], $r^{(ss)}\equiv r(t\to\infty)=\lim_{s\to 0^+}[s\tilde{r}(s)]$. The steady-state solution of Eqs. (2a)–(2e) can then be computed directly as $\vec{r}^{(ss)}=-A^{-1}(s\to 0^+)\vec{b}$.

The $s\to 0^+$ limit of the kernel function in LT space is given by Eq. (B12) and repeated below:

$$\tilde{K}(\delta)\equiv\tilde{K}(s\to 0^+;\delta)=\begin{cases} -i\dfrac{\beta^{3/2}}{\sqrt{\delta_g-\delta}}, & \delta_g-\delta>0, \\ \dfrac{\beta^{3/2}}{\sqrt{|\delta_g-\delta|}}, & \delta_g-\delta<0. \end{cases} \tag{3}$$

The interpretation of the quantity $\tilde{K}(\delta)$ is given as follows: for $\delta_g-\delta<0$ or equivalently $\omega_{be}<\omega_{32}+\delta$ the 3-2 transition lies in the allowed propagating frequency region of the photonic crystal (Fig. 2). β, given explicitly by Eq. (B7b) (again with $\{nmlp\}=\{3223\}$), can be thought of as a diagonal decay rate modified by the structured vacuum near the PBE (where $\beta\sim\omega_{32}^{7/2}$ while the usual spontaneous emission rate varies as $\gamma\sim\omega_{32}^3$). Though the presence of the inverse square root at first sight appears to make this modified decay rate diverge at $\delta_g=\delta$, in any rationalized expression, the square-root factors can be arranged so that the denominator of any physical quantity is finite and the square roots appear in the numerator in such a way as to indicate the frequency "cutoff" for this modified spontaneous emission. For the opposite limit $\delta_g-\delta>0$ the frequency $\omega_{32}+\delta$ lies completely in the PBG (nonpropagating photon region). The modified decay ceases, and $\tilde{K}(\delta)$ acts instead as a dispersive term—i.e., the well-known frequency shifts induced by the PBE [12].

An inspection of Eqs. (2d) and (2e) reveals that they (and their complex conjugates) form a homogeneous set of equations in steady-state that decouple from the remaining components and therefore $r_{21}^{(ss)}=r_{32}^{(ss)}=0$. The remaining set of equations (2a)–(2c) are easily solved by matrix inversion for their steady-state values $\{r_{22}^{(ss)},r_{33}^{(ss)},r_{31}^{(ss)}\}$:

$$r_{22}^{(ss)}=\frac{[\tilde{K}(0)+\tilde{K}^*(0)]|\Omega_p|^2(\Delta_-+\Delta_-^*)}{D}, \tag{4a}$$

$$r_{33}^{(ss)}=\frac{2\gamma_2|\Omega_p|^2(\Delta_-+\Delta_-^*)}{D}, \tag{4b}$$

$$r_{31}^{(ss)}=\frac{i2\gamma_2\Omega_p\Delta_-^*\{2\gamma_3+[\tilde{K}(0)+\tilde{K}^*(0)]\}}{D}, \tag{4c}$$

where

$$\Delta_-=i\Delta_p-[\gamma_3+\tilde{K}(\Delta_p)],$$

$$D=[4\gamma_2+\tilde{K}(0)+\tilde{K}^*(0)]|\Omega_p|^2(\Delta_-+\Delta_-^*)-2\gamma_2|\Delta_-|^2[2\gamma_3+\tilde{K}(0)+\tilde{K}^*(0)]. \tag{5}$$

Of particular interest is the material polarization $P_{31}^{(ss)}=\Omega_p r_{31}^{(ss)}$ whose imaginary part gives the absorption profile for the probe field and whose real part gives the index of refraction.

B. Limiting forms of the steady-state solutions

We now consider several different limiting forms of the exact steady-state solutions of Eqs. (4a)–(4c). In the limit of a weak probe $\Omega_p\ll\gamma_3$ we expand the above solutions to first order in Ω_p/γ_3 to obtain

$$r_{22}^{(ss)}=r_{33}^{(ss)}=0, \tag{6a}$$

$$r_{31}^{(ss)}=-i\frac{\Omega_p}{\Delta_-}=\frac{-\Omega_p}{\Delta_p+i[\gamma_3+\tilde{K}(\Delta_p)]}. \tag{6b}$$

Note that the above steady-state solutions are independent of the value of any assumed damping rate γ_2 from level 2 to 1.

The expression for $r_{31}^{(ss)}$ above is the same solution obtained by Paspalakis *et al.* [see [5], Eq. (10)] with $\Omega_p\to-\Omega$, $\Delta_p\to\delta$, and $\gamma_3\to\gamma/2$ obtained in a weak-probe-field Wigner-Weisskopf-like solution in the Schrödinger picture with a wave function of the form (translating to our three-level atom notation)

$$|\psi(t)\rangle=a_1(t)|1,\{0\}\rangle+a_3(t)e^{-i\Delta_p t}|3,\{0\}\rangle,+\sum_{\vec{k},\lambda}a_{\vec{k}\lambda}(t)|2,\{\vec{k}\lambda\}\rangle \tag{7}$$

and Hamiltonian

$$H = -\Omega_p e^{i\Delta_p t}|1\rangle\langle 3| - i\gamma_3|3\rangle\langle 3| + \sum_{\vec{k},\lambda} c_{\vec{k}\lambda} e^{-i(\omega_{\vec{k}}-\omega_{31})t}|3\rangle\langle 2|\hat{a}_{\vec{k}\lambda} + \text{H.c.} \tag{8}$$

In the above $|i,\{0\}\rangle$ is the atom in state $|i\rangle$ with no photons in the field and $|2,\{\vec{k}\lambda\}\rangle$ is the atom in state $|2\rangle$ with a single photon of arbitrary momentum and polarization in the field. Substituting the above expressions into the Schrödinger equation $i|\dot{\psi}\rangle = H|\psi\rangle$ and formally eliminating the amplitudes $a_{\vec{k}\lambda}(t)$ yields the equations

$$i\dot{a}_1(t) = \Omega_p a_3(t), \tag{9a}$$

$$i\dot{a}_3(t) = \Omega_p a_1(t) - \{\Delta_p + i[\gamma_3 + K(t;\Delta_p) \star]\}a_3(t). \tag{9b}$$

Under the assumption of a weak probe field Ω_p such that $a_1(t) \approx 1$ for all times, Eq. (9b) yields the exact same solution as Eq. (6b) when one notes that

$$r_{31}(t) = a_3(t)a_1^*(t) \approx a_3(t), \quad \text{for } a_1(t) \approx 1. \tag{10}$$

In fact, Eq. (2c) for $r_{31}(t)$ becomes exactly Eq. (9b) for $a_3(t)$ if we set $r_{22}(t) = r_{33}(t) = 0$ in the former, appropriate for the weak-probe assumption $a_1(t) \approx 1$ for all times. In Fig. 3(a) we illustrate the absorption and dispersion profile for Eq. (4c) in the weak-probe limit of $\Omega_p/\gamma_3 = 0.1$ which should be compared with Fig. (1a) in Paspalakis *et al.* [5]. The notable feature here is the simultaneous zero in the absorption and emission curves (termed "transparency" in [5]) which results from a factor of $\sqrt{|\delta_g - \Delta_p|}$ in the numerator of the polarization arising from modification of the decay rates in the vicinity of the PBE. In Fig. 3(b) we increase the probe field strength by a factor of 10 to $\Omega_p/\gamma_3 = 1.0$. The resulting plots show the effects of power broadening due to the probe and are beginning to approach the free-space absorption and dispersion profiles for the transition from level 3 to 1. In Figs. 4 and 5 we illustrate the effects of a negative and positive detuning, respectively, of the PBE from level 3 [compare to Figs. 2(a) and 2(c), respectively of [5]]. The absorption and dispersion curves are essentially identical to the $\delta_g = 0$ case, since the previously discussed factor of $\sqrt{|\delta_g - \Delta_p|}$ in the material polarization determines the position of the simultaneous zero in the absorption and dispersion curves. The (b) figures indicate how power broadening changes the corresponding weak-field (a) figure results.

A further inspection of Eqs. (4a)–(4c) reveals that for $\gamma_2 \equiv 0$ (e.g., if levels 1 and 2 have the same parity and we ignore dephasing effects), $D(\gamma_3 \to 0) = [\tilde{K}(0) + \tilde{K}^*(0)]|\Omega_p|^2(\Delta_- + \Delta_-^*)$ so that $r_{33}^{(ss)} = r_{31}^{(ss)} = 0$ and $r_{22}^{(ss)} = 1$. Thus, if there is no dipole-allowed transition from level 2 to 1, eventually all population is transferred from level 1 to level 2, regardless of the probe field intensity, in contrast to the weak-field results of Eqs. (6a) and (6b).

Finally, for $\delta_g > 0$ or $\omega_{be} > \omega_{32}$ the 3-2 transition lies completely in the PBG, implying that $\tilde{K}^*(0)$ is the complex conjugate of $\tilde{K}(0)$ so that their sum is identically zero. Equation (4c) then yields

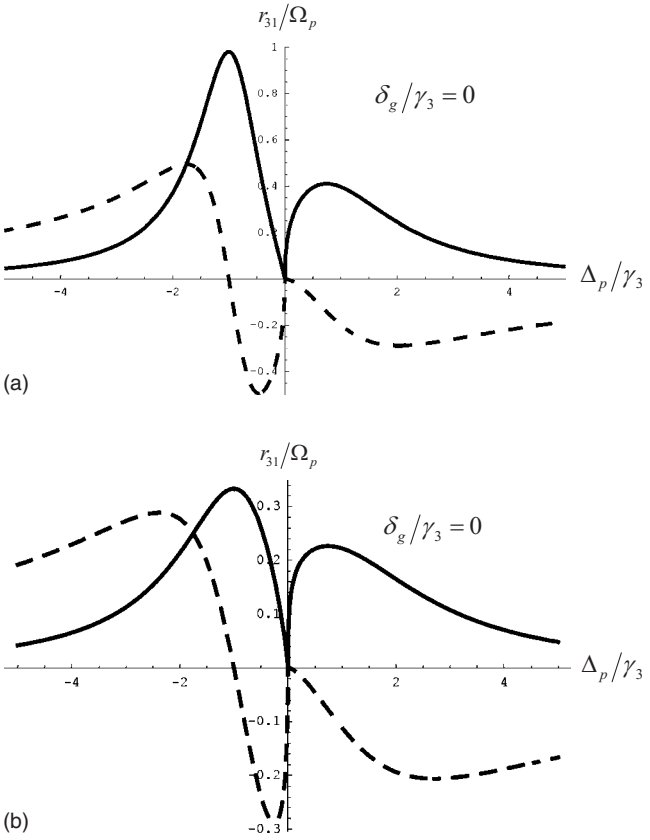

FIG. 3. Steady-state solution of $r_{31}^{(ss)}/\Omega_p$ from Eq. (4c) as a function of Δ_p/γ_3. The solid curves are the absorption profiles (in arbitrary units), and the dashed curves are the index of refraction $(n-1)$. (a) Weak-probe limit: $\gamma_3 \equiv 1$, $\gamma_2 = 0.02$, $\beta = 1.0$, $\Omega_p = 0.1$, and $\delta_g = \omega_{be} - \omega_{32} = 0$ [compare with Fig. (1a) of [5]]. (b) Same parameters as above, except for $\Omega_p = 1.0$, showing power-broadening effects due to the increased probe field strength.

$$r_{31}^{(ss)} = -i\frac{\Omega_p}{\Delta_-}\frac{1}{\left[1 - \frac{|\Omega_p|^2}{\gamma_3}\left(\frac{1}{\Delta_-} + \frac{1}{\Delta_-^*}\right)\right]}, \tag{11}$$

which is again independent of γ_2 [which is not true in general if $\delta_g < 0$—i.e., ω_{32} in the propagating photon region above ω_{be}; see Eqs. (4a)–(4c)]. The second factor in the square brackets in Eq. (11) indicates the power-broadening effects of the modified damping from level 3 to 1 when this transition lies completely in the PBG [compare with Eq. (6b)].

III. EIT NEAR A PBE

In this section we consider the addition of a strong-coupling field E_c of frequency ω_c between levels 2 and 3, with detuning $\Delta_c = \omega_c - \omega_{32}$, in the atomic system discussed in the previous section (see Fig. 1). This leads to the widely explored effect of EIT in which the absorption and dispersion of a weak probe, again from levels 1 to 3, is modified by the presence of the coupling field with Rabi frequency Ω_c between levels 2 and 3 [8,13]. The distinguishing characteristic

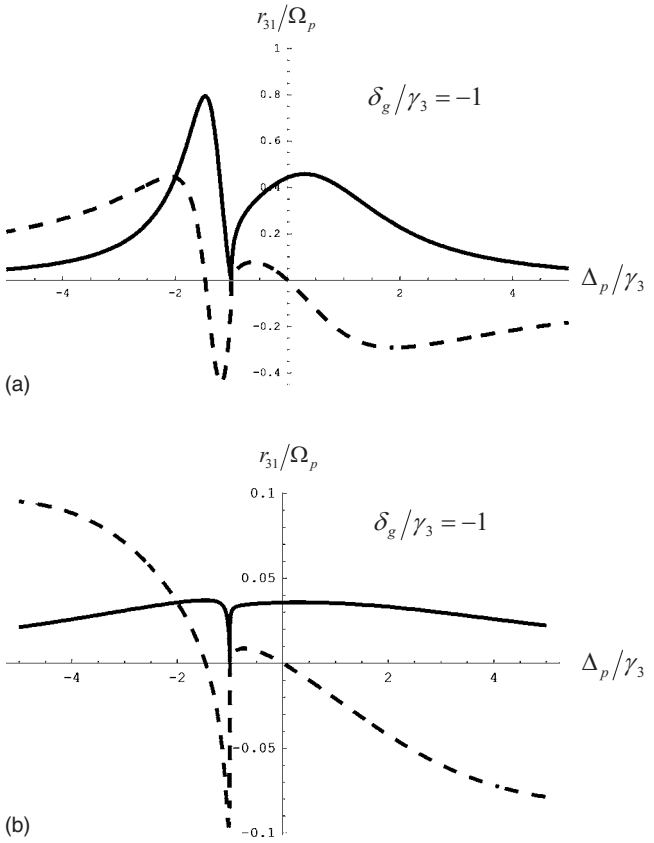

FIG. 4. Steady-state solution of $r_{31}^{(ss)}/\Omega_p$ from Eq. (4c) as a function of Δ_p/γ_3. The solid curves are the absorption profiles (in arbitrary units), and the dashed curves are the index of refraction, with same parameters as Fig. 3 except with $\delta_g=\omega_{be}-\omega_{32}=-1$: (a) Weak-probe limit: $\Omega_p=0.1$. (b) $\Omega_p=1.0$, showing power-broadening effects due to the increased probe field strength.

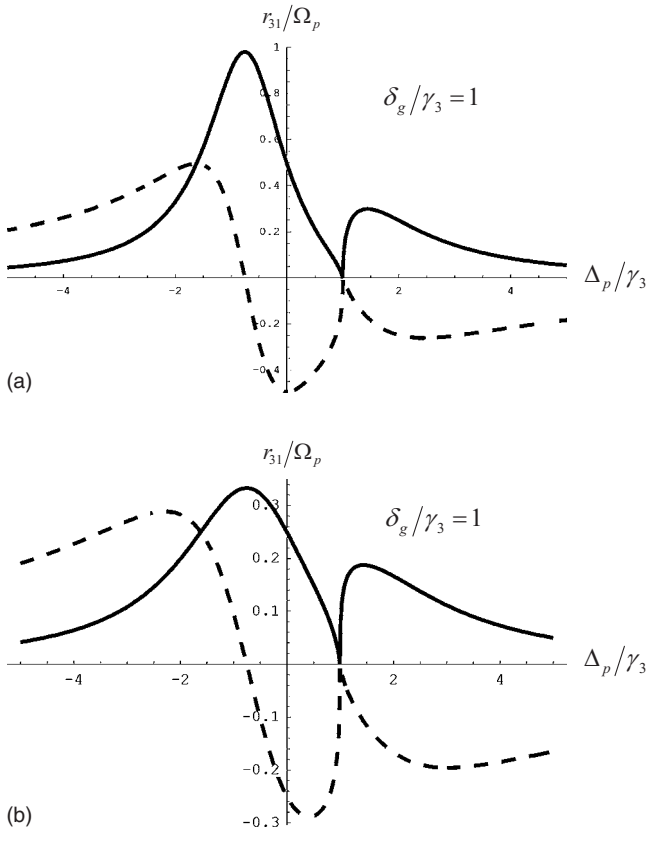

FIG. 5. Steady-state solution of $r_{31}^{(ss)}/\Omega_p$ from Eq. (4c) as a function of Δ_p/γ_3. The solid curves are the absorption profiles (in arbitrary units), and the dashed curves are the index of refraction, with same parameters as Fig. 3 except with $\delta_g=\omega_{be}-\omega_{32}=1$: (a) Weak-probe limit: $\Omega_p=0.1$. (b) $\Omega_p=1.0$, showing power-broadening effects due to the increased probe field strength.

of EIT is the zero (or near-zero) absorption profile on (or near) probe resonance $\Delta_p=0$, with a corresponding zero of the index of refraction. This is illustrated in Fig. 6 for EIT in free space with a control detuning of $\Delta_c/\gamma_3=0.1$, in the usual weak-field limit which treats the populations $r_{22}(t)$ and $r_{33}(t)$ as negligible, as well as the coherence $r_{32}(t)$. This leads to the coupled set of equations for the coherences r_{31} and r_{21} [13]

$$\dot{r}_{31} = [i\Delta_p - \gamma_3]r_{31} + i\Delta_c r_{21} + i\Delta_p, \tag{12a}$$

$$\dot{r}_{21} = [i(\Delta_p - \Delta_c) - \gamma_2]r_{21} + i\Delta_c r_{31}, \tag{12b}$$

with solution

$$r_{31}^{(ss)} = -\frac{\Omega_p[\ (\Delta_p - \Delta_c) + i\gamma_2)]}{(\Delta_p + i\gamma_3)(\Delta_p - \Delta_c + i\gamma_2) - \Omega_c^2}. \tag{13}$$

The absorption minimum is exactly zero if $\gamma_2 \equiv 0$. In general the 1-2 transition is dipole forbidden and γ_2 represents a dephasing rate, which is typically very small. The condition for EIT is that $\Omega_c^2 \gg \gamma_2\gamma_3$. For a nonzero Δ_c the minimum of the absorption profile occurs at $\Delta_p \approx (1-\gamma_2/\gamma_3)\Delta_c$. The absorption maxima occur at roughly $\Delta_p \approx \pm\Omega_c$ (exactly where the Stark-split doublet levels occur). By varying Ω_c while still maintaining the EIT condition, one can adjust the steepness of the index of refraction near the absorption minimum. This leads to very small group velocities and to the phenomenon of slow light [13,14].

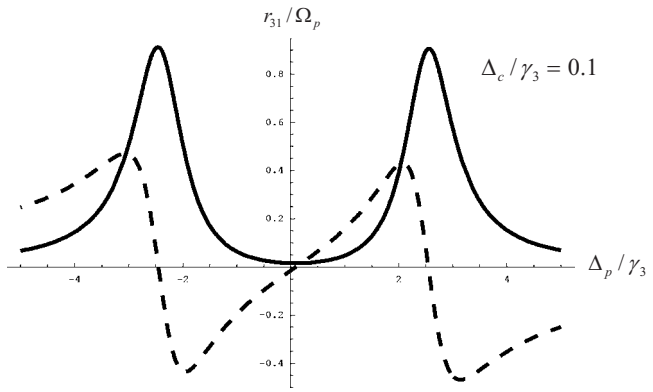

FIG. 6. Steady-state solution of $r_{31}^{(ss)}/\Omega_p$ as a function of Δ_p/γ_3 for EIT in free space [from Eqs. (14a)–(14e) with $\beta \to 0$] for parameters $\gamma_3=1$, $\gamma_2=0.02$, $\Omega_c=2.5$, and $\Delta_c=0.1$. Solid curve: absorption profile (in arbitrary units). Dashed curve: index of refraction $(n-1)$.

We can easily modify Eqs. (2a)–(2e) to include the coupling field Ω_c [using Eq. (A17)]. The EIT equations of motion in the presence of a PBE are then given by

$$\dot{r}_{22}(t) = i\Omega_c^* r_{32} - i\Omega_c r_{23} - 2\gamma_2 r_{22}(t) + [K_{32}(t;0) + K_{32}^*(t;0)] \star r_{33}(t), \tag{14a}$$

$$\dot{r}_{33}(t) = -\{2\gamma_3 + [K_{32}(t;0) + K_{32}^*(t;0)] \star\} r_{33}(t) + i\Omega_p r_{13}(t) - i\Omega_p^* r_{31}(t) + i\Omega_c r_{23} - i\Omega_c^* r_{32}, \tag{14b}$$

$$\dot{r}_{31}(t) = \{i\Delta_p - [\gamma_3 + K_{32}(t;\Delta_p) \star]\} r_{31}(t) + i\Omega_p [r_{11}(t) - r_{33}(t)] + i\Omega_c r_{21}, \tag{14c}$$

$$\dot{r}_{21}(t) = \{i(\Delta_p - \Delta_c) - [\gamma_2 + K_{23}(t;\Delta_p - \Delta_c) \star]\} r_{21}(t) - i\Omega_p r_{23}(t) + i\Omega_c^* r_{31}, \tag{14d}$$

$$\dot{r}_{32}(t) = \{i\Delta_c - [\gamma_2 + \gamma_3 + K_{32}(t;\Delta_c) \star]\} r_{32}(t) + i\Omega_c (r_{22} - r_{33}) + i\Omega_p r_{12}(t). \tag{14e}$$

In the weak-field limit, we obtain the same form of the solution for $r_{31}^{(ss)}$ as in Eq. (13), but now with the substitutions

$$\gamma_2 \to \bar{\gamma}_2 = \gamma_2 + \tilde{K}_{23}(\Delta_p - \Delta_c),$$

$$\gamma_3 \to \bar{\gamma}_3 = \gamma_3 + \tilde{K}_{32}(\Delta_p). \tag{15}$$

In Fig. 7 we show the alteration of the EIT phenomenon when the 2-3 transition is zero detuned from the PBE by $\delta_g = \omega_{be} - \omega_{32} = 0$, with the same parameters that were used in the free-space case in Fig. 6. In these figures we plot the real and imaginary parts of the susceptibility r_{31}/Ω_p in the weak-field limit, treating $r_{22}(t) = r_{33}(t) = r_{23}(t) \approx 0$. In Fig. 7(a), $\Delta_c/\gamma_3 = 0.1$ such that $\delta_g - \Delta_c < 0$. This implies that the coupling field $E_c e^{i\omega_c t} + \text{c.c.}$ with frequency ω_c lies in the propagating region of the PhC. Thus, for probe detunings $\Delta_p \ll \delta_g - \Delta_c$ the EIT absorption and dispersion profiles are essentially unaltered.

For $\Delta_p \gg \delta_g - \Delta_c$ the presence of the PBE reduces the absorption and dispersion features relative to their free-space profiles. Near the PBE $\Delta_p \approx \delta_g$ a new absorption and dispersion feature arises, Fig. 7(b), that is reminiscent of PBE-distorted profiles in Fig. 3(a). Again, there is a zero in both the absorption and dispersion profiles at $\Delta_p = \delta_g$, due to the rationalization of the square-root factors from the kernel functions $\tilde{K}(\delta)$ in Eq. (3), leading to an overall factor of $\sqrt{|\Delta_p - \delta_g|}$ in the numerator for these expressions.

The EIT absorption and dispersion features are very sensitive to the value of the detuning $\delta_g - \Delta_c$. In Figs. 7(a) and 7(b), $\delta_g - \Delta_c < 0$ so that the coupling frequency ω_c lies in the propagating region of the PhC. In Fig. 7(c), we choose $\Delta_c/\gamma_3 = -0.1$ so that $\delta_g - \Delta_c > 0$. This now implies that ω_c lies completely within the PBG, so that this frequency does not propagate in the PhC. Hence, for $\delta_g > 0$ we set $\Omega_c = 0$ in our solutions. Since the 2-3 transition lies within the PBG, the EIT effect is destroyed and the PBE-distorted 1-3 transition absorption and dispersion profiles remain, which are now just essentially Fig. 3(a).

In Fig. 8 we use the same parameters as in Fig. 7, but now with $\delta_g/\gamma_3 = -1$. Since level 3 lies outside the PBG, these figures are very similar to Figs. 7(a) and 7(b). In Fig. 9 the parameters are again as in Fig. 7, but now with $\delta_g/\gamma_3 = 1$. Since level 3 now lies within the PBE such that ω_c is in the nonpropagating region of the PhC, we again obtain the PBE-distorted 1-3 transition absorption and dispersion profiles of Figs. 7(c) and 3(a).

IV. FIELD-INDUCED TRANSPARENCY NEAR A PBE

We now consider a three-level atom in which levels 2 and 3 are close enough that their separate transitions to level 1 can coherently interfere (Fig. 10) and that $\mu_{32} = 0$ (e.g., levels 2 and 3 are of the same parity, which is opposite that of level 1). This effect, first studied by Cardimona *et al.* [9] in 1982 and called "field-induced transparency" was a precursor to the widely studied electromagnetically induced transparency [8]. While EIT considers a three-level atom in the Λ configuration with a probe field on levels 1 to 3 and a coupling field on levels 2 to 3, FIT considers the three-level atom in the V configuration illustrated in Fig. 10 where the two closely spaced excited levels are coupled by a single probe field. (In EIT, the Stark-split doublet created by the coupling field takes the place of these closely spaced excited states).

Mathematically, the closeness of levels 2 and 3 leads us to consider ω_{32} as a small (nonoptical) frequency such that $e^{i\omega_{32}t}$ is treated as a slowly varying quantity in the RWA and we set $\rho_{32}(t) = r_{32}(t)$. The time dependences of the remaining density matrix elements are given by $\rho_{ii}(t) = r_{ii}(t)$, $\rho_{31}(t) = r_{31}(t)e^{-i\omega_p t}$, and $\rho_{21}(t) = r_{21}(t)e^{-i\omega_p t}$, and probe detuning is now defined as $\Delta_p = \omega_p - \omega_{21}$. Again we assume that all the population is initially in the ground state, $r_{11}(t=0) = 1$. We further assume that both transition frequencies ω_{31} and ω_{21} are on the order of the band-edge frequency ω_{be} and define $\delta_g = \omega_{be} - \omega_{21}$ (see Fig. 10).

In free space the FIT equations take the form [9]

$$\dot{r}_{22}(t) = -2\gamma_2 r_{22}(t) - i\Omega_p^* r_{21}(t) - \gamma_{23}^* r_{32}(t) + i\Omega_p r_{12}(t) - \gamma_{23} r_{23}(t), \tag{16a}$$

$$\dot{r}_{33}(t) = -2\gamma_3 r_{33}(t) - i\Omega_{p'}^* r_{31}(t) - \gamma_{32} r_{32}(t) + i\Omega_{p'} r_{13}(t) - \gamma_{32}^* r_{23}(t), \tag{16b}$$

$$\dot{r}_{31}(t) = i\Omega_{p'}[r_{11}(t) - r_{33}(t)] - \gamma_{32}^* r_{21}(t) + [i(\Delta_p - \omega_{32}) - \gamma_3] r_{31}(t) - i\Omega_p r_{32}(t), \tag{16c}$$

$$\dot{r}_{21}(t) = i\Omega_p[r_{11}(t) - r_{22}(t)] - \gamma_{23}^* r_{31}(t) + (i\Delta_p - \gamma_2) r_{21}(t) - i\Omega_{p'} r_{23}(t), \tag{16d}$$

$$\dot{r}_{32}(t) = -\gamma_{32}^* r_{22}(t) - \gamma_{23} r_{33}(t) - [i\omega_{32} + (\gamma_2 + \gamma_3)] r_{32}(t) - i\Omega_p^* r_{31}(t) + i\Omega_{p'} r_{12}(t), \tag{16e}$$

where we again drop all small (Lamb) frequency shift terms. In the above we have introduced the shorthand notation for

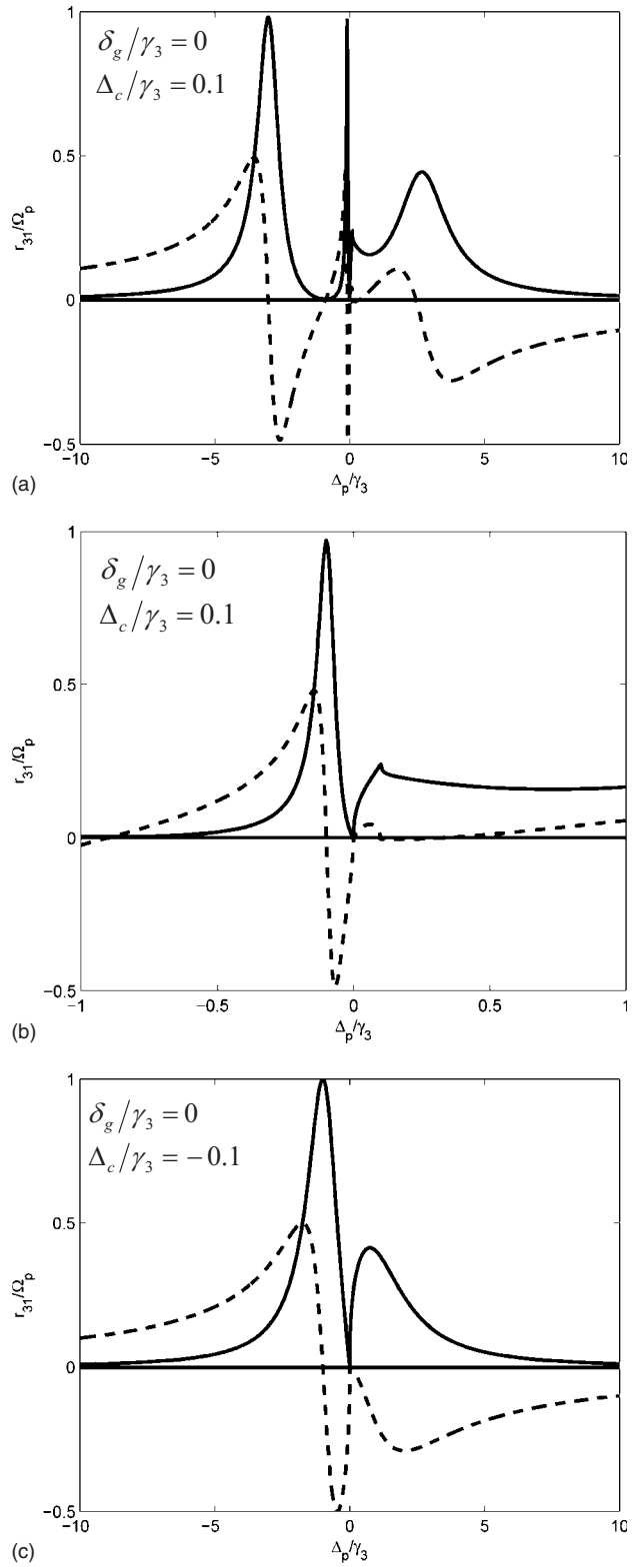

FIG. 7. EIT near a PBE: r_{31}/Ω_p (a) absorption (solid line) and index of refraction (dashed line) with parameters $\gamma_3 \equiv 1$, $\delta_g = 0$, $\gamma_2 = 0.02$, $\beta = 1$, $\Omega_c = 2.5$, $\Delta_c = 0.1$ with $\delta_g - \Delta_c < 0$ so that coupling field $E_c e^{-i\omega_c t}$ with frequency ω_c is in the propagating region of the PhC, (b) enlargement of features near PBE in (a), (c) Same parameters as in (a) except that $\Delta_c = -0.1$ so that $\delta_g - \Delta_c > 0$. Now the control field E_c at frequency ω_c lies in the PBG, and therefore cannot propagate.

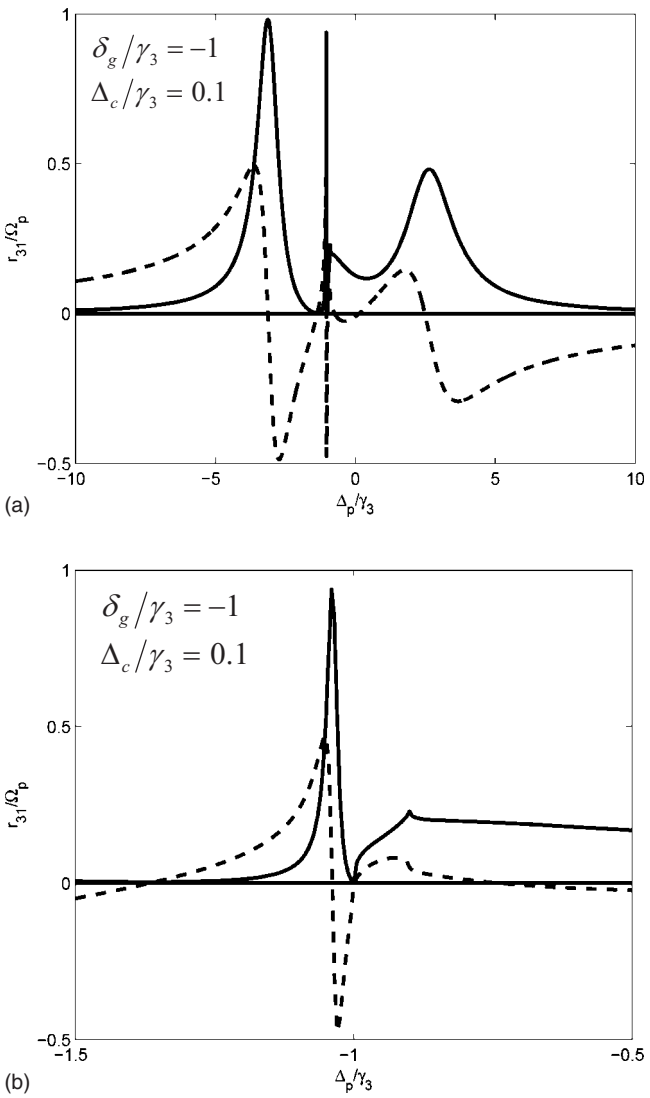

FIG. 8. EIT near a PBE: r_{31}/Ω_p (a) absorption (solid line) and index of refraction (dashed line) with same parameters as in Fig. 7(a), but now with $\delta_g = -1$ ($\delta_g - \Delta_c < 0$). (b) Enlargement of features near PBE in (a).

the generalized damping rates $\gamma_2 \equiv \gamma_{2112}$, $\gamma_3 \equiv \gamma_{3113}$, $\gamma_{23} \equiv \gamma_{2113}$, and $\gamma_{32} \equiv \gamma_{3112}$ where from, from Eq. (A13), $\gamma_{nmlp} \propto \omega_{nm}\omega_{pl}\vec{\mu}_{nm}\cdot\vec{\mu}_{lp}\Theta(\omega_{pl})$. The solution of the above FIT equations yields a characteristic destructive interference pattern in the absorption profile when the probe is tuned in between levels 2 and 3 as shown in Fig. 11. The steady-state susceptibility χ which is proportional to polarization

$$\chi^{(ss)} \sim P^{(ss)} = \Omega_p r_{21}^{(ss)} + \Omega_{p'} r_{31}^{(ss)}, \tag{17}$$

where $\Omega_p = (\vec{\mu}_{21}\cdot\vec{e}_L)E_L/\hbar$ and $\Omega_{p'} = (\vec{\mu}_{31}\cdot\vec{e}_L)E_L/\hbar$ display an interference numerator $2\gamma_2|\Omega_p|^2[(z^2+1)\Delta_p - \omega_{32}]^2$ for the absorption and a corresponding numerator proportional to $\Delta_p[(z^2+1)\Delta_p - \omega_{32}](\Delta_p - \omega_{32})$ for the index of refraction, where z has been defined as the ratio of the magnitude of the dipole moments from the ground state to levels 2 and 3, $\mu_{31} = z\mu_{21}$.

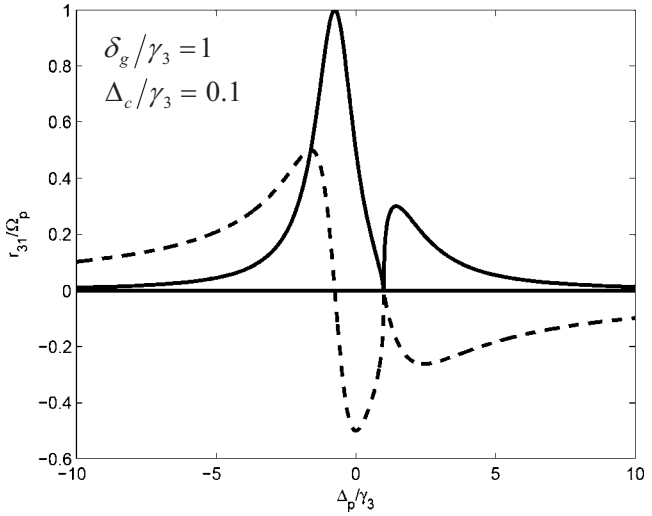

FIG. 9. EIT near a PBE: r_{31}/Ω_p (a) absorption (solid line) and index of refraction (dashed line) with same parameters as in Fig. 7(a) but now with $\delta_g=1$ ($\delta_g-\Delta_c>0$). The control field E_c at frequency ω_c lies in the PBG and therefore cannot propagate.

In the presence of a PBE, the FIT equations of motion are modified to

$$\dot{r}_{22}(t) = -[K_2(t;0) + K_2^*(t;0)]\star r_{22}(t) - i\Omega_p^* r_{21}(t) - K_{23}(t;0)\star r_{32}(t) + i\Omega_p r_{12}(t) - K_{23}^*(t;0)\star r_{23}(t), \tag{18a}$$

$$\dot{r}_{33}(t) = -[K_3(t;\omega_{32}) + K_3^*(t;\omega_{32})]\star r_{33}(t) - i\Omega_{p'}^* r_{31}(t) - K_{23}^*(t;\omega_{32})\star r_{32}(t) + i\Omega_{p'} r_{13}(t) - K_{23}(t;\omega_{32})\star r_{23}(t), \tag{18b}$$

$$\dot{r}_{31}(t) = i\Omega_{p'}[r_{11}(t) - r_{33}(t)] - K_{23}(t;\Delta_p)\star r_{21}(t) + [i(\Delta_p - \omega_{32}) - K_3(t;\Delta_p)\star] r_{31}(t) - i\Omega_p r_{32}(t), \tag{18c}$$

$$\dot{r}_{21}(t) = i\Omega_p[r_{11}(t) - r_{22}(t)] - K_{23}(t;\Delta_p)\star r_{31}(t) + [i\Delta_p - K_2(t;\Delta_p)\star] r_{21}(t) - i\Omega_{p'} r_{23}(t), \tag{18d}$$

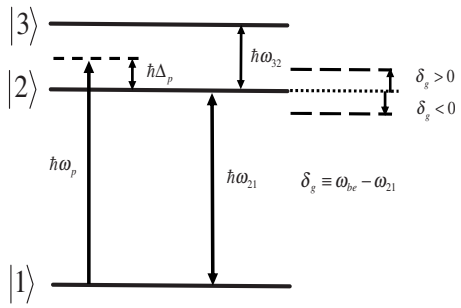

FIG. 10. Same energy level diagram as in Fig. 1 but now with levels 2 and 3 close enough (nonoptical) that their emission to level 1 can coherently interfere. This is the FIT configuration considered by Cardimona *et al.* [9], now modified by the presence of a PBE.

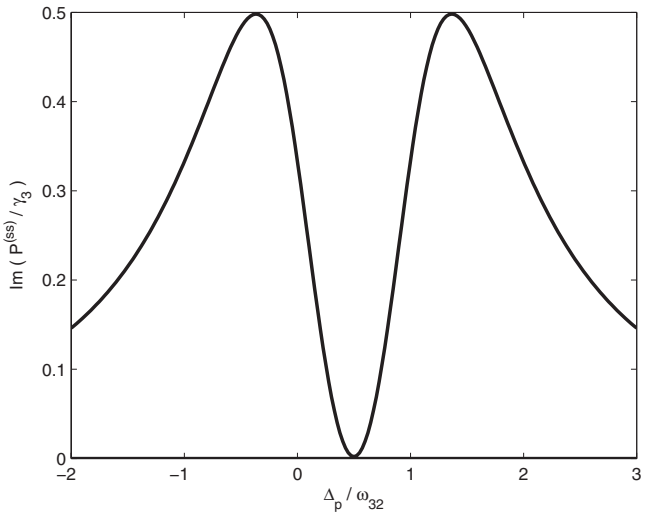

FIG. 11. Absorption profile from the steady-state material polarization $P^{(ss)}=\Omega_p r_{21}^{(ss)}+\Omega_{p'} r_{31}^{(ss)}$ of the FIT equations of motion in free space (no PBG) [9].

$$\dot{r}_{32}(t) = -K_{23}(t;0)\star r_{22}(t) - K_{23}^*(t;\omega_{32})\star r_{33}(t) - \{i\omega_{32} + [K_2^*(t;\omega_{32}) + K_3(t;0)]\star\} r_{32}(t) - i\Omega_p^* r_{31}(t) + i\Omega_{p'} r_{12}(t), \tag{18e}$$

where again $r_{11}+r_{22}+r_{33}=1$. In the above equations we have used the shorthand notation $K_2(t;0)\equiv K_{2112}(t;0)$, $K_3(t;0)\equiv K_{3113}(t;0)$, $K_{23}(t;\delta)\equiv K_{2113}(t;\delta)$, and $K_{32}(t;\delta)\equiv K_{3112}(t;\delta)$ for $\delta\in\{0,\Delta_p,\omega_{32}\}$. Again these equations can be solved via LTs for their steady-state values as a linear set of algebraic equations. We see that for $s\to 0^+$, the LT quantities $\tilde{K}_2(0)+\tilde{K}_2^*(0)$ and $\tilde{K}_3(\omega_{32})+\tilde{K}_3^*(\omega_{32})$ [see Eq. (3)] generalize the diagonal decay rates γ_2 and γ_3, respectively, in the vicinity of a PBE. The quantities $\tilde{K}_{23}(\Delta)$ and $\tilde{K}_{32}(\Delta)$ generalize the "off-diagonal" cooperative decay rates γ_{2113} and γ_{3112}, respectively, that are crucial for the destructive interference effects between the dipole emission from levels 3 to 1 and level 2 to 1 that gives rise to the FIT effect in Fig. 11. Although the steady-state solutions to Eqs. (18a)–(18e) can be written down in closed form, their general form are not particularly illuminating. We can observe, however, that for weak pumping, in which we set $r_{22}^{(ss)}=r_{33}^{(ss)}=0$, the density matrix components $r_{21}^{(ss)}$, $r_{31}^{(ss)}$, and $r_{32}^{(ss)}$ and their complex conjugates form a closed set of coupled equations. Hence the steady-state material polarization, Eq. (17), depends intimately on the coherence $r_{32}^{(ss)}$ developed between levels 2 and 3.

In Fig. 12 we show the effects of the PBE on the absorption profile for $\delta_g=\omega_{be}-\omega_{21}=-0.35\omega_{32}$, so that both transitions from levels 2 and 3 to the ground state lie in the propagating photon region of the PhC (see Fig. 10). Note that all frequencies are now normalized to the separation frequency ω_{32}. Further, for $\Delta_p<\delta_g$, the probe frequency ω_p would lie within the PBG and we must set $\Omega_p\equiv 0$. In Fig. 12 the absorption profile has the same form as its free-space value in Fig. 11 except that it exhibits a sharp turn-on once $\Delta_p>\delta_g$.

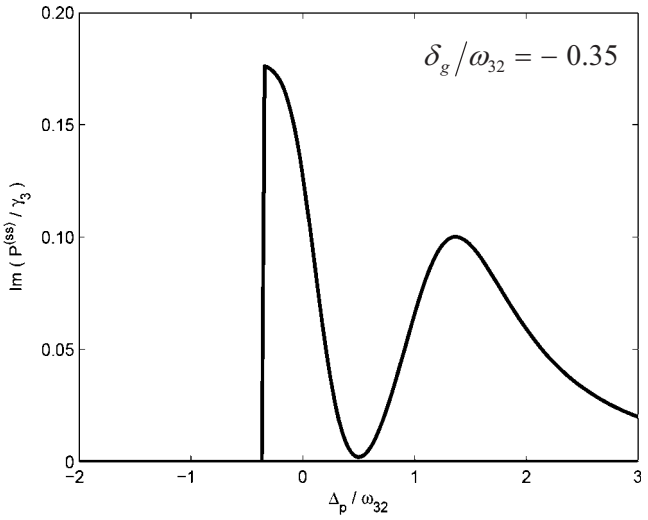

FIG. 12. Absorption profile from the steady-state polarization $P^{(ss)}=\Omega_p r_{21}^{(ss)}+\Omega_{p'} r_{31}^{(ss)}$ of the FIT equations of motion near a PBG for $\omega_{32}\equiv 1$, $\delta_g=-0.35\omega_{32}$, $z=1$, $\Omega_p=0.50$, $\Omega_{p'}=z\Omega_p$, $\beta_2=0.050$, $\beta_3=z^2\beta_2$, and $\beta_{32}=z\beta_2$ appropriate for $\mu_{31}=z\mu_{21}$.

The factor $\sqrt{|\delta_g-\Delta_p|}$, arising in the numerator due to the PBE, merely adds a zero at $\Delta_p=\delta_g$ to the null values for the material polarization which already occur for $\Delta_p<\delta_g$.

In Fig. 13 we show the effects of the PBE on the absorption profile for $\delta_g=0.35\omega_{32}$, so that now level 2 lies within the PBG, while level 3 lies in the propagating photon region (see Fig. 10). Since δ_g is now greater than zero, the PBE-modified diagonal decay rate from level 2 $[\tilde{K}_2(0)+\tilde{K}_2^*(0)]$ in Eq. (18a) sums exactly to zero since each term is purely imaginary from Eq. (3). Further, all terms of the form $\tilde{K}(0)$ switch from purely real for $\delta_g<0$ to purely imaginary for $\delta_g>0$. Formally, Eqs. (18a)–(18e) yield an exact, yet unphysical solution in which all steady-state values of $r_{ji}^{(ss)}$ are purely real, with $r_{33}^{(ss)}=-r_{32}^{(ss)}$, and the polarization, in the case

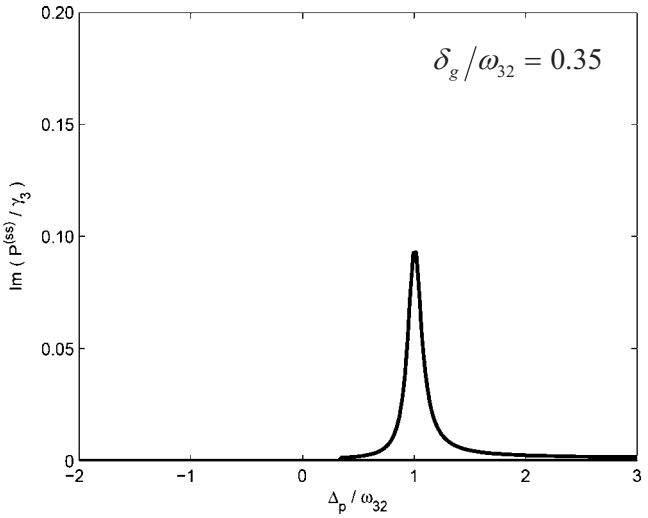

FIG. 13. Steady-state polarization $P^{(ss)}=\Omega_p r_{21}^{(ss)}+\Omega_{p'} r_{31}^{(ss)}$ with same values as Fig. 12, except with $\delta_g=0.35\omega_{32}$.

$z\equiv 1$, is identically zero—i.e., $r_{21}^{(ss)}+r_{31}^{(ss)}=0$. The unphysical nature of this solution arises since nonradiative decay rates from levels 2 and 3 to level 1, as well as coherence dephasing rates, have been omitted from our derivation. Ordinarily these nonradiative decay rates are very small in magnitude compared to the diagonal decay rates $[\tilde{K}_2(0)+\tilde{K}_2^*(0)]$ from level 2 to level 1 and $[\tilde{K}_3(\omega_{32})+\tilde{K}_3^*(\omega_{32})]$ from level 3 to level 1 when $\delta_g<0$. Consequently, we have included small phenomenological diagonal decay terms $-2\gamma_{(nr)}r_{ii}(t)$ and dephasing terms $-\gamma_{(nr)}r_{ji}(t)$ to the FIT equations, where $\gamma_{(nr)}$ is a factor of 10^3 smaller than the radiative diagonal decay rates. As shown in Fig. 13 this yields the expected single-transition absorption line shape centered on level 3 at $\Delta_p=\omega_{32}$. The FIT interference effect has been wiped out since level 2 now lies completely within the PBG and is thus inhibited from radiating.

Last, for $\delta_g>\omega_{32}$ (and $\Delta_p>\delta_g$ in order that the probe can propagate in the PhC), the PBE-modified diagonal decay rates $[\tilde{K}_2(0)+\tilde{K}_2^*(0)]$ from level 2 to level 1 and $[\tilde{K}_3(\omega_{32})+\tilde{K}_3^*(\omega_{32})]$ from level 3 to level 1 become identically zero, since both transitions now lie within the PBG. Formally, the system undergoes pure Rabi oscillations between the ground and excited states. However, with the inclusion of small nonradiative decay rates from both excited levels, we obtain a truncated version of the absorption profile in Fig. 13 centered about $\Delta_p=\delta_g$, though drastically reduced in magnitude.

As a pure quantum interference phenomenon, FIT can be understood as depending crucially on the additional coherence-assisted decay of one of the excited levels due to the other excited level. In a photonic crystal these decay rates are modified by the presence of the PBE. For the case $\delta_g<0$ all PBE-modified decay rates are real, $\tilde{K}(\delta)=\beta^{3/2}/\sqrt{|\delta_g-\delta|}$ [see Eq. (3)] for $\delta\in\{0,\Delta_p,\omega_{32}\}$. In this case, the equations for FIT near a PBE, Eqs. (18a)–(18e), are formally analogous to the free-space FIT equations (16a)–(16e) with modified decay rates. There are two classes of decay rates: diagonal as illustrated in Fig. 14 and off-diagonal as illustrated in Fig. 15. Considering first the diagonal decay rates (Fig. 14), the terms $\tilde{K}_3(\omega_{32})$ and $\tilde{K}_2(0)$ indicate "direct" radiative decay from levels 3 and 2, respectively. The terms $\tilde{K}_3(\Delta_p)$ and $\tilde{K}_2(\Delta_p)$ indicate photon-assisted decay from the power-broadened linewidths due to the probe. Last, $\tilde{K}_3(0)$ indicates a decay from level 3 resulting from a coherent coupling to level 2, which damps the coherence r_{32} via the population in level 3 [replacing $-\gamma_3 r_{32}$ in Eq. (16e) in the free-space FIT equations]. Similarly, $\tilde{K}_2(\omega_{32})$ indicates the corresponding process of a decay from level 2 resulting from a coherent coupling to level 3, which damps the coherence r_{32} via the population in level 2 [replacing $-\gamma_2 r_{32}$ in Eq. (16e)].

In Fig. 15 we illustrate the off-diagonal decay terms. Again, there are decay rates $\tilde{K}_{23}(\Delta_p)$ and $\tilde{K}_{23}(\Delta_p)$ indicating photon-assisted decay of level 2 or 3 due to level 3 or 2, respectively, arising from the presence of the probe. In addition, there are cross-coherence coupling terms such as $\tilde{K}_{23}(0)$ and $\tilde{K}_{23}(0)$ indicating the decay of level 3 due to a coherent

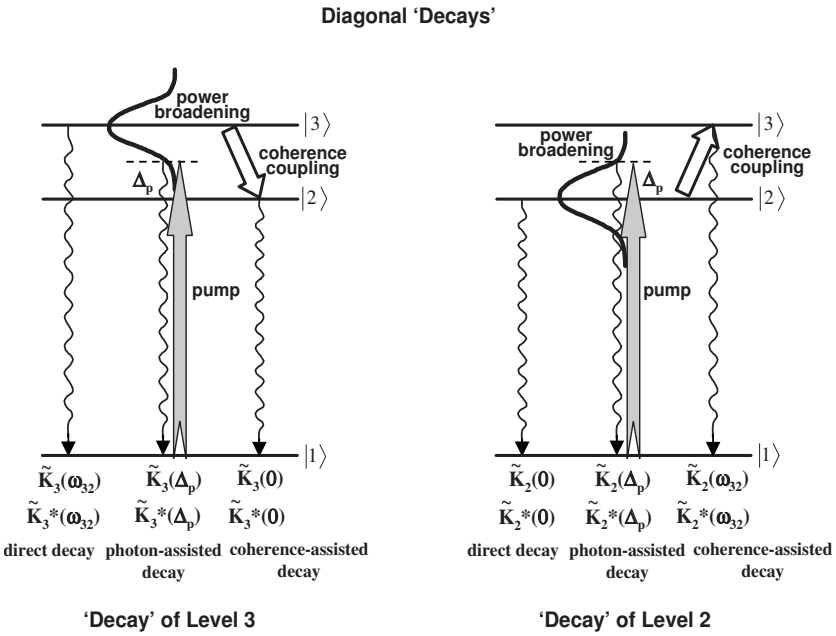

FIG. 14. FIT: diagonal decay rates. See Eqs. (3) and (18a)–(18e) and discussion in text.

coupling with level 2 and the corresponding terms $\tilde{K}_{23}(\omega_{32})$ and $\tilde{K}_{23}(\omega_{32})$ indicating the decay of level 2 due to a coherent coupling with level 3.

When δ_g becomes greater than zero and the lower excited level 2 lies completely within the PBG, the decay rate $\tilde{K}(\delta_g)$ changes character from a formerly real decay rate ($\delta_g < 0$) to a purely imaginary "decay rate." The most significant consequence of this occurrence is that level 2 can no longer radiatively decay. Hence the FIT destructive interference phenomenon is destroyed, resulting in a single-transition radiative decay from level 3 alone, although the coherence r_{32} between level 3 outside and level 2 inside the PBG still persists.

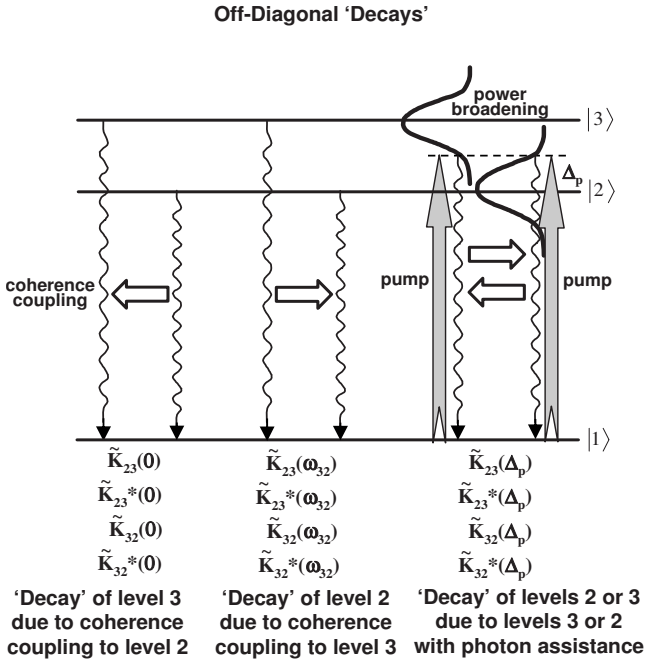

FIG. 15. FIT: off-diagonal decay rates. See Eqs. (3) and (18a)–(18e) and discussion in text.

V. SUMMARY AND CONCLUSIONS

In this work we have explored spontaneous emission and quantum interference effects in the vicinity of a PBE. We have formulated a set of density matrix equations in which the integrals involving the atom-field interactions governing the emitted dipole radiation are computed explicitly for a model of the photon dispersion relation valid near the PBE. The formulation of the atom-field equations of motion presented in this work differs from the conventional Schrödinger approach in which the wave function is considered to have components containing at most one (or a few) photons. Our approach allows us to consider probe and driving fields of arbitrary strength and atoms with an arbitrary number of levels. The model of the PBG structure used in this work was 3D and isotropic for ease of exposition, and could easily be extended to nonisotropic models.

We considered a three-level atom, with a probe from the ground to the highest excited level, in three different configurations: (i) the transition frequency of the upper two excited levels ω_{32} in the optical regime, (ii) the previous configuration but now with a coupling field between the upper two levels, and (iii) the transition frequency of the upper two levels on the order of the linewidths of each of the levels. In the first two cases, the transition frequency between the ground state and highest excited level was considered to be much greater than the width of the PBG and hence occurs as if in free space, while the transition frequency of the upper two levels was near the band-edge frequency ω_{be}. In the last case, the PBG had a width on the order of the ground to excited transitions, the latter of which were spaced close enough that their dipole emissions could coherently interfere.

For all three cases, the relevant parameter was the detuning of a radiative transition from the band-edge frequency:

$\delta_g=\omega_{be}-\omega_{32}$ in the first two cases and $\delta_g=\omega_{be}-\omega_{21}$ in the last case. For $\delta_g<0$, the uppermost level (3) lay outside the PBG in cases (i) and (ii) and hence the kernel function (in Laplace transform space, at $s=0$) $\tilde{K}$ acted like a (real) damping rate modified by the presence of the PBE. For $\delta_g>0$, the uppermost level lay within the PBG and $\tilde{K}$ changed character to a purely imaginary quantity, thus contributing a dispersive or frequency shift effect. In the last case (iii), the sign of δ_g determined if the lowest excited level (2) was inside or outside of the PBG.

We used our density matrix equations to explore EIT in the vicinity of a PBE [case (ii) above]. In addition, we also explored the effects of the PBE on FIT [case (iii) above)], which demonstrates a purely quantum destructive interference effect between the dipole radiation of the two closely spaced upper levels. In future work we will explore the addition of a cavity within the photonic crystal and its effects upon the above quantum interference effects.

ACKNOWLEDGMENT

This research was supported by the Air Force Office of Scientific Research (AFOSR).

APPENDIX A: DERIVATION OF DENSITY MATRIX EQUATIONS FOR SPONTANEOUS EMISSION NEAR A PHOTONIC BAND EDGE

1. Free-space equations

Following Milonni and Smith [7] we derive the general interaction between a quantized electromagnetic field and a single atom consisting of an arbitrary number of levels. The Hamiltonian is given by

$$H = H_A + H_F + H_{AF}, \tag{A1}$$

where the Hamiltonians for the atom (H_A), the field (H_F), and the light-matter interaction (H_{AF}) are given by

$$H_A = \frac{p^2}{2m_e} + V(r), \tag{A2a}$$

$$H_F = \sum_{\vec{k},\lambda} \hbar\omega_k a^\dagger_{\vec{k}\lambda} a_{\vec{k}\lambda}, \tag{A2b}$$

$$H_{AF} = -\frac{e}{m_e c}\vec{A}(0,t)\cdot\vec{p} + \frac{e^2}{2m_e c^2}\vec{A}^2(0,t). \tag{A2c}$$

In the above, m_e is the mass of the electron, $a_{\vec{k}\lambda}$ is the photon annihilation operator for wave vector $\vec{k}$ and polarization λ, and we have invoked the dipole approximation in which the field has been evaluated at the site of the nucleus. In what follows we ignore, as usual, the $\vec{A}^2(0,t)$ term in Eq. (A2c). In the Heisenberg picture, we define the (fixed) initial atomic state $|n(0)\rangle \equiv |n\rangle$ at $t=0$ for the nth energy eigenstate of H_A. We define the Heisenberg atomic operator σ_{ij} as

$$\sigma_{ij}(t) = e^{iHt/\hbar}\sigma_{ij}(0)e^{-iHt/\hbar},$$

where $\sigma_{ij}(0)=|i\rangle\langle j|$. We then obtain

$$\vec{p}(t) = \sum_m \sum_n \langle n|\vec{p}(0)|m\rangle\sigma_{nm}(t) = -\frac{im_e}{e}\sum_m \sum_n \omega_{mn}\vec{\mu}_{nm}\sigma_{nm}(t), \tag{A3}$$

where $\hbar\omega_{nm}=E_n-E_m$ and $\vec{\mu}_{nm}=\langle n|e\vec{r}(0)|m\rangle$ is the electric-dipole moment transition matrix element between states n and m. The equal-time commutators of the atomic operators are given by

$$[\sigma_{ij}(t),\sigma_{mn}(t)] = \delta_{jm}\sigma_{in}(t) - \delta_{ni}\sigma_{mj}(t), \tag{A4}$$

where $\sigma_{ij}(t)\sigma_{mn}(t)=\delta_{jm}\sigma_{in}(t)$ has been used.

The Hamiltonian H in Eq. (A1) is given by

$$H = \sum_n E_n\sigma_{nn}(t) + \sum_{\vec{k},\lambda}\hbar\omega_{\vec{k}}a^\dagger_{\vec{k}\lambda}(t)a_{\vec{k}\lambda}(t) + i\hbar\sum_{\vec{k},\lambda}\sum_{n,m} C_{\vec{k}\lambda nm}\sigma_{nm}(t) \times[a^\dagger_{\vec{k}\lambda}(t) + a_{\vec{k}\lambda}(t)], \tag{A5}$$

where the atom-field coupling constants are given by

$$C_{\vec{k}\lambda nm} = \frac{1}{\hbar}\left(\frac{2\pi\hbar}{\omega_{\vec{k}}V}\right)^{1/2}\omega_{mn}\vec{\mu}_{nm}\cdot\vec{e}_{\vec{k}\lambda}, \tag{A6}$$

where $\vec{e}_{\vec{k}\lambda}$ is the polarization vector of the electric field taken to be real (linear polarization basis) [15].

Choosing normal ordering, in which photon creation operators are placed to the extreme left and photon annihilation operators are placed to the extreme right, the Heisenberg equations of motion $i\hbar\dot{\eta}(t)=[\eta(t),H]$ for the operator $\eta(t)$ are given by

$$\dot{a}_{\vec{k}\lambda}(t) = -i\omega_{\vec{k}}a_{\vec{k}\lambda} + \sum_{mn} C_{\vec{k}\lambda nm}\sigma_{nm}(t), \tag{A7a}$$

$$\dot{\sigma}_{ij}(t) = \sum_{\vec{k},\lambda}\sum_{mn} C_{\vec{k}\lambda nm}[\delta_{jn}\sigma_{im}(t) - \delta_{im}\sigma_{nj}(t)]a_{\vec{k}\lambda} + \sum_{\vec{k},\lambda}\sum_{mn} C_{\vec{k}\lambda nm}a^\dagger_{\vec{k}\lambda}[\delta_{jn}\sigma_{im}(t) - \delta_{im}\sigma_{nj}(t)]. \tag{A7b}$$

Formally integrating Eq. (A7a) yields

$$a_{\vec{k}\lambda}(t) = a_{\vec{k}\lambda}(0)e^{-i\omega_{\vec{k}}t} + \sum_{mn} C_{\vec{k}\lambda nm}\int_0^t dt' e^{-i\omega_{\vec{k}}(t-t')}\sigma_{nm}(t'), \tag{A8}$$

where $a_{\vec{k}\lambda}(0)e^{-i\omega_{\vec{k}}t}$ represents the free electromagnetic field, which we will take as a classical probe, and the remaining integral in Eq. (A8) represents the radiation reaction field due to the radiating atomic dipoles.

Substituting Eq. (A8) into Eq. (A7b) yields the equation of motion for the atomic operators $\sigma_{ij}(t)$. The radiating dipole (second) term in Eq. (A8) yields the following atomic decay contributions to Eq. (A7b):

$$\dot{\sigma}_{ij}|_{decay} = \sum_{\vec{k},\lambda} \sum_{nmlp} C_{\vec{k}\lambda nm} \times \left\{ C_{\vec{k}\lambda lp} [\delta_{jn}\sigma_{im}(t) - \delta_{im}\sigma_{nj}(t)] \times \int_0^t dt' e^{-i\omega_{\vec{k}}(t-t')}\sigma_{lp}(t') + \text{H.c.} \right\}. \tag{A9}$$

For the free vacuum, with dispersion relation $\omega_{\vec{k}}=|\vec{k}|c$, the integral in Eq. (A9) is handled in the usual way [7]: assuming the atom-field interaction is weak, the atomic dipoles nearly evolve according to their free evolution $\dot{\sigma}_{nm}(t) = i\omega_{nm}\sigma_{nm}(t)$. Thus, one can make the "adiabatic approximation"

$$\sigma_{nm}(t') \cong \sigma_{nm}(t)e^{-i\omega_{nm}(t-t')}, \tag{A10}$$

or $\sigma_{nm}(t')e^{-i\omega_{nm}t'} = \sigma_{nm}(t)e^{-i\omega_{nm}t}$ states that both sides of the latter equality are slowly varying quantities in time. Equation (A10) allows one to pull $\sigma_{lp}(t')$ outside the time integral and evaluate it at time t. The resulting time integral over the exponential phase factor is treated in the usual Wigner-Weisskopf "pole" approximation

$$\int_0^t dt' e^{-i(\omega_{\vec{k}}-\omega_{pl})(t-t')} \cong \pi\delta(\omega_{\vec{k}} - \omega_{pl}) - i\,\mathrm{P}\left[\frac{1}{\omega_{\vec{k}} - \omega_{pl}}\right], \tag{A11}$$

where "P" stands for the "principal part" integral. The remain mode summation over $\vec{k}\lambda$ can be performed in the continuum limit utilizing $\Sigma_{\vec{k},\lambda} \to \Sigma_\lambda V/(2\pi)^3 \int d^3k$ to yield

$$\dot{\sigma}_{ij}|_{decay} = -\sum_{nmlp} \Gamma_{nmlp}(\omega_{pl}) \times [\delta_{jn}\sigma_{im}(t) - \delta_{im}\sigma_{nj}(t)]\sigma_{lp}(t) + \text{H.c.}, \tag{A12}$$

where the atomic operators at the same time t can now be combined to yield, for example, $\sigma_{im}(t)\sigma_{lp}(t) = \delta_{ml}\sigma_{ip}(t)$ and where we have defined

$$\Gamma_{nmlp}(\omega_{pl}) \cong \frac{2\omega_{nm}\omega_{pl}^2}{3\hbar c^3}\vec{\mu}_{nm}\cdot\vec{\mu}_{lp}\Theta(\omega_{pl}) - i\frac{2\omega_{nm}\omega_{pl}}{3\pi\hbar c^3}\vec{\mu}_{nm}\cdot\vec{\mu}_{lp}\,\mathrm{P}\int_0^\infty \frac{d\omega\omega}{(\omega-\omega_{pl})} \equiv \gamma_{nmlp} - i\Delta_{nmlp}. \tag{A13}$$

In the above γ_{nmlp} represents an "off-diagonal" cooperative decay [7,9] between levels n to m and p to l, which is proportional to the scalar product of their respective dipole moments, Δ_{nmlp} represents a cooperative "Lamb shift," and $\Theta(\omega_{pl})$ is the Heaviside unit-step function indicating that we have nonzero decay if and only if $p>l$. In this work, we ignore the Lamb shifts, but will retain the "off-diagonal" decay terms. The usual "diagonal" decay terms from level n to m occur for $p=n$, $l=m$.

2. Formulation of equations near a PBE

Instead of pulling $\sigma_{lp}(t')$ outside the time integral in Eq. (A9), we could have equivalently "pushed" the atomic operators at time t inside the integral, using the adiabatic approximation in the form

$$\sigma_{nm}(t) \cong \sigma_{nm}(t')e^{i\omega_{nm}(t-t')}, \tag{A14}$$

so that for example we would have

$$\sigma_{im}(t)\int_0^t dt' e^{-i\omega_{\vec{k}}(t-t')}\sigma_{lp}(t') \cong \int_0^t dt' e^{-i(\omega_{\vec{k}}-\omega_{im})(t-t')}\sigma_{im}(t')\sigma_{lp}(t') = \delta_{ml}\int_0^t dt' e^{-i(\omega_{\vec{k}}-\omega_{im})(t-t')}\sigma_{ip}(t'). \tag{A15}$$

Although, at first sight Eq. (A15) appears unnecessarily complicated, this form will be shown in the next section to be much more useful when we consider the structured vacuum in the neighborhood of a PBE with a nontrivial dispersion relation $\omega_{\vec{k}}=\omega(\vec{k})$. Further, Eq. (A15) is a convolution integral appearing in the equation for $\dot{\sigma}_{ij}(t)$ which can be easily handled in a solution method utilizing Laplace transforms.

We note that the adiabatic approximation assumes that the atom-field interaction is weak. Formally this approximation is invalid near the photonic band edge ω_{be} where the density of states diverges. However, we can avoid this divergence by introducing a level-broadening parameter [16] based on the long, but constant average finite lifetime τ of the field modes in any realistic photonic crystal. The density of states would then be given by

$$\rho(\omega) \sim \begin{cases} \dfrac{1}{\sqrt{\omega-\omega_{be}}}, & \omega > \omega_{be} + 1/\tau, \\ \sqrt{\tau}, & \omega_{be} < \omega < \omega_{be} + 1/\tau. \end{cases}$$

The constant, finite density of states for $\omega_{be}<\omega<\omega_{be}+1/\tau$ allows us to invoke the adiabatic approximation, which to lowest order assumes that the atomic operators evolve essentially freely by H_A or, more accurately, that $\sigma_{nm}(t)e^{-i\omega_{nm}t}$ is a slowly varying quantity. The adiabatic approximation is then valid in Eqs. (A10) and (A15) since the atom-field (dipole) coupling constants $C_{\vec{k}\lambda nm}$ are weak and the corrections are of higher order. In the following we ignore this technical detail and treat τ as infinite, since all sums over modes and integrals over time can be computed exactly in this limit.

We can convert the Heisenberg equations of motion for $\dot{\sigma}_{ij}(t)$ into density matrix equations utilizing $\rho_{ji}(t)=\langle\sigma_{ij}(t)\rangle$, where the expectation value is taken with respect to the Heisenberg state $|\psi(0)\rangle = |\psi\rangle_A \otimes |\alpha\rangle_F$ where $|\psi\rangle_A$ is the initial atomic state and $|\alpha\rangle_F$ is a coherent state, representing the free electric field of the probe laser:

$$\vec{E} = E_L e^{-i\omega_p t}\vec{e}_L + \text{c.c.}, \tag{A16}$$

where we take E_L real and $\vec{e}_L$ complex. The density matrix equations are then given by

$$\dot{\rho}_{ji}(t) = -i\omega_{ji}\rho_{ji} + \sum_n [\Omega_{jn}\rho_{ni}(t) - \rho_{jn}\Omega_{ni}(t)] + \int_0^t dt' \left\{ \left[\sum_{\vec{k},\lambda} C_{\vec{k}\lambda jl} C_{\vec{k}\lambda lp} e^{-i(\omega_{\vec{k}}-\omega_{il})(t-t')} \right] \rho_{pi}(t') - \left[\sum_{\vec{k},\lambda} C_{\vec{k}\lambda li} C_{\vec{k}\lambda jp} e^{-i(\omega_{\vec{k}}-\omega_{lj})(t-t')} \right] \rho_{pl}(t') + \left[\sum_{\vec{k},\lambda} C_{\vec{k}\lambda jl} C^*_{\vec{k}\lambda ip} e^{i(\omega_{\vec{k}}+\omega_{il})(t-t')} \right] \rho_{lp}(t') - \left[\sum_{\vec{k},\lambda} C_{\vec{k}\lambda li} C^*_{\vec{k}\lambda lp} e^{i(\omega_{\vec{k}}+\omega_{lj})(t-t')} \right] \rho_{jp}(t') \right\}, \quad \text{(A17)}$$

where we have defined $\Omega_{ij}=\vec{\mu}_{ij}\cdot\vec{E}_L/\hbar$. Note that in Eq. (A17) the RWA has not yet been made. In the next Appendix we will perform the mode sum over $\vec{k}\lambda$ when certain atomic transitions are near a PBE.

APPENDIX B: EVALUATIONS OF MODE SUMS NEAR A PBE

In this Appendix we will perform the mode sums appearing in the density matrix equation Eq. (A17) and derive the equations of motion for the slowly varying components of the density matrix used in the body of the paper. This is best illustrated for the specific case of the three-level atom discussed in Sec. II (see Fig. 1), where we considered the transition between levels 2 and 3 to be optically separated and near a PBE and a ground-state level 1 far from the PBE. For this system we write the density matrix elements $\rho_{ji}(t)$ in terms of the slowly varying time components $r_{ji}(t)$ as $\rho_{ii}(t)=r_{ii}(t)$, $\rho_{31}(t)=r_{31}(t)e^{-i\omega_p t}$, $\rho_{21}(t)=r_{21}(t)e^{-i(\omega_p-\omega_{32})t}=r_{21}(t)e^{-i(\omega_{21}+\Delta_p)t}$, and $\rho_{32}(t)=r_{32}(t)e^{-i\omega_{32}t}$ and their complex conjugates. Here ω_p is the frequency of the laser probe field and $\Delta_p=\omega_p-\omega_{31}$ is the detuning from the upper level 3. Additionally, levels 2 and 3 are far enough apart that $e^{-i\omega_{32}t}$ is considered a rapidly varying term. In the following, we make the RWA and drop rapidly oscillating frequencies.

1. Diagonal damping terms

As a concrete example, we consider the damping terms for $\rho_{22}(t)=r_{22}(t)$ from Eq. (A17) in the RWA. The terms in the first and fourth square brackets for $l=1$ and $p=2$ yield the following integral that contributes to the atomic damping:

$$\dot{r}_{22}(t) \sim 2\int_0^t dt' \sum_{\vec{k},\lambda} C_{\vec{k}\lambda 21} C_{\vec{k}\lambda 12} e^{-i(\omega_{\vec{k}}-\omega_{21})(t-t')} r_{22}(t'). \quad \text{(B1)}$$

Since ω_{21} lies far from the PBE, we can treat this term as in Appendix A by using the Markov approximation and evaluating the slowing varying term $r_{22}(t')$ at the upper limit of the integration, $r_{22}(t')\cong r_{22}(t)$. The remaining temporal integral is the same as considered in Eq. (A11), and the resulting mode sum yields

$$\dot{r}_{22}(t) \sim -\gamma_{2112} r_{22}(t) \equiv -\gamma_2 r_{22}(t),$$

which is the usual "diagonal damping" term considered in Appendix A [recall that $C_{\vec{k}\lambda 21}C_{\vec{k}\lambda 12}\sim(-\omega_{21})(-\omega_{12})=-(\omega_{12})^2$ which gives rise to the minus sign above].

2. Damping near the PBE

In addition to the usual damping terms above for transitions far from the PBE, there exist contributions in Eq. (A17) arising from transitions near the PBE. The terms in the second set of square brackets in Eq. (A17) with $l=p=3$ give rise to the contribution

$$\dot{r}_{22}(t) \sim \int_0^t dt' \sum_{\vec{k},\lambda} C_{\vec{k}\lambda 23} C_{\vec{k}\lambda 32} e^{-i(\omega_{\vec{k}}-\omega_{32})(t-t')} r_{33}(t'), \quad \text{(B2)}$$

while the terms in the third set of square brackets for $l=p=3$ give rise to the contribution

$$\dot{r}_{22}(t) \sim \int_0^t dt' \sum_{\vec{k},\lambda} C_{\vec{k}\lambda 23} C^*_{\vec{k}\lambda 32} e^{i(\omega_{\vec{k}}-\omega_{32})(t-t')} r_{33}(t'). \quad \text{(B3)}$$

For the isotropic dispersion relation considered in this paper we have [see Eq. (1)] the quadratic dispersion relation valid near the PBE:

$$\omega_{\vec{k}} = \omega_k = \omega_{be} + A(|\vec{k}| - |\vec{k}_0|)^2, \quad A = c^2/\omega_g, \quad \text{(B4)}$$

where ω_{be} is the frequency of the PBE, ω_g is the frequency width of the gap, and $k_0=|\vec{k}_0|=\omega_g/c$. The above dispersion relation is valid for $\omega_g \gg c(|\vec{k}|-|\vec{k}_0|)$. For the transition frequency between levels 2 and 3 near the PBE, $\delta_g=\omega_{be}-\omega_{32}$ is considered as a slowly varying frequency, and hence we perform the mode sum in Eq. (B2) explicitly, to find the effects of the structure vacuum on the atomic decay. We do this as follows [3]: the sum over polarizations λ can be performed explicitly as in Appendix A [7]. Going to the continuum limit for the wave vector $\vec{k}$ yields the following integral (after performing the angular integration):

$$e^{i\delta_g(t-t')} \int_0^\infty dk \frac{k^2}{\omega_k} e^{-iA(k-k_0)^2(t-t')}. \quad \text{(B5)}$$

The integral over k in Eq. (B5) is treated in the stationary-phase approximation where we replace $k\to k_0$ in all terms except in the argument of the exponential [10]. The remaining integral over a complex Gaussian can converted to an elementary real Gaussian integral with the following simple change of variables $x=e^{-i\pi/4}\sqrt{A}k$. Equation (B2) is then evaluated as the convolution integral

$$\dot{r}_{22}(t) \sim \int_0^t dt' K_{2332}(t-t';0) r_{33}(t'), \quad \text{(B6)}$$

where for an arbitrary frequency detuning δ

$$K_{nmlp}(t-t';\delta) = \beta_{nmlp}^{3/2} \frac{e^{-i[\pi/4-(\delta_g-\delta)(t-t')]}}{\sqrt{t-t'}}, \quad \text{(B7a)}$$

$$\beta_{nmlp}^{3/2} = \frac{|\omega_{nm}||\omega_{lp}|\omega_{be}\sqrt{\omega_g}\vec{\mu}_{nm}\cdot\vec{\mu}_{lp}}{12\pi^{3/2}c^3\hbar\epsilon_0}, \tag{B7b}$$

valid for $t>t'$. Since all frequencies in Eq. (B7b) are nearly the same, one often sees the expression $\beta_{nmlp}^{3/2}\to\beta^{3/2}\sim|\omega_{nm}|^{7/2}$ in the literature [3,5].

Equation (B3) gives the complex-conjugate contribution of Eq. (B6) so that the equation for $r_{22}(t)$ is given by

$$\dot{r}_{22}(t) = -\gamma_{21}r_{22}(t) + [K_{2332}(t;0) + K_{2332}^{*}(t;0)]\star r_{33}(t), \tag{B8}$$

where $\star$ indicates the convolution operator $A(t)\star B(t) = \int dt' A(t-t')B(t')$.

A similar analysis for the equation of motion for $\rho_{31}(t) = r_{31}(t)e^{-i\omega_p t}$ reveals that there is a diagonal decay term $-\gamma_{31}r_{31}(t)$ due to the transition from level 3 to 1, which lies far from the PBE. In addition, there is a contribution $-K_{3223}(t;\Delta_p)\star r_{31}(t)$, arising from the term in the first set of square brackets in Eq. (A17) with $l=2$ and $p=3$, which gives rise to an integral of the form

$$\dot{r}_{31}(t) \sim \int_0^t dt' \sum_{\vec{k},\lambda} C_{\vec{k}\lambda 32}C_{\vec{k}\lambda 23}e^{-i[\omega_{\vec{k}}-(\omega_p-\omega_{21})](t-t')}r_{31}(t'). \tag{B9}$$

Since $\omega_p-\omega_{21}=\omega_{32}+\Delta_p$, this gives rise to a slowly varying frequency $\delta_g-\Delta_p$ in the exponential, which is again treated as non-Markovian, since this frequency is small and in the neighborhood of the PBE.

Finally, in considering the solution to the equations of motion for $r_{ji}(t)$ we will employ LTs and utilize the well-known fact that the LT of a convolution is a product of the LT of the individual functions in the integrand. The LT of $K_{nmlp}(t)$ is an elementary integral which is easily performed (utilizing the change of variables $t\to x^2$), yielding

$$\tilde{K}_{nmlp}(s;\delta) \equiv \int_0^\infty dt e^{-st}K_{nmlp}(t) = \beta_{nmlp}^{3/2}\frac{e^{-i\pi/4}}{\sqrt{s+i(\delta_g-\delta)}}. \tag{B10}$$

In particular, for the steady-state solutions we use the well-known long-time-limit theorem of Laplace transforms:

$$r(t\to\infty) = \lim_{s\to 0^+}[s\tilde{r}(s)], \tag{B11}$$

where $\tilde{r}(s)$ is the LT of $r(t)$. In particular, we will need the $s\to 0^+$ limit of Eq. (B10). Taking the branch cut of the square root to lie along the negative real s axis so that $-1=e^{-i\pi}$ we obtain

$$\tilde{K}(\delta) \equiv \tilde{K}_{nmlp}(s\to 0^+;\delta) = \begin{cases} -i\dfrac{\beta_{nmlp}^{3/2}}{\sqrt{\delta_g-\delta}}, & \delta_g-\delta>0, \\ \dfrac{\beta_{nmlp}^{3/2}}{\sqrt{|\delta_g-\delta|}}, & \delta_g-\delta<0. \end{cases} \tag{B12}$$

Thus, for $\delta_g-\delta<0$ or equivalently $\omega_{be}<\omega_{32}+\delta$ the 3-2 transition lies in the allowed propagating frequency region of the photonic crystal. $\tilde{K}(\delta)$ can be thought of as a diagonal decay rate modified by the structured vacuum near the PBE (recall $\beta\sim\omega_{32}^{7/2}$ while the usual spontaneous emission rate varies as $\gamma\sim\omega_{32}^{3}$). Though the presence of the inverse square root at first sight appears to make this modified decay rate diverge at $\delta_g=\delta$, in any rationalized expression, the square-root factors can be arranged so that the denominator of any physical quantity is finite and the square roots appear in the numerator in such a way as to indicate the "cutoff" for this modified spontaneous emission. For the opposite limit $\delta_g-\delta>0$ the frequency $\omega_{32}+\delta$ lies completely in the PBG (nonpropagating photon region). The modified decay ceases and $\tilde{K}(\delta)$ acts instead as a dispersive term—i.e., the well-known frequency shifts induced by the PBE [12].

[1] P. Lambropoulos, G. M. Nikolopoulos, T. R. Nielsen, and S. Bay, Rep. Prog. Phys. **63**, 455 (2000).

[2] P. W. Milonni, *The Quantum Vacuum* (Cambridge University Press, New York, 1976).

[3] S. John and J. Wang, Phys. Rev. Lett. **64**, 2418 (1990); S. John and T. Quang, Phys. Rev. A **50**, 1764 (1994); Phys. Rev. Lett. **74**, 3419 (1995); N. Vats and S. John, Phys. Rev. A **58**, 4168 (1998).

[4] A. Yariv and P. Yeh, *Optical Waves in Crystals* (Wiley, New York, 1984).

[5] E. Paspalakis, N. J. Kylstra, and P. L. Knight, Phys. Rev. A **60**, R33 (1999).

[6] G. M. Nikolopoulos and P. Lambropoulos, Phys. Rev. A **61**, 053812 (2000).

[7] P. W. Milonni and W. A. Smith, Phys. Rev. A **11**, 814 (1975).

[8] S. E. Harris, Phys. Rev. Lett. **62**, 1033 (1989); M. Fleischhauer, A. Imamoglu, and J. P. Marangos, Rev. Mod. Phys. **77**, 633 (2005).

[9] A. Cardimona, M. G. Raymer, and C. R. Stroud, J. Phys. B **15**, 55–64 (1982).

[10] Our work is easily extended to the anisotropic PBG model with dispersion relation of the form $\omega_{\vec{k}}=\omega_{be}+A(\vec{k}-\vec{k}_0)^2$ with a density of states that varies as $\rho(\omega)\sim\Theta(\omega-\omega_{be})\sqrt{\omega-\omega_{be}}$ (see [3,5]). However, here we will only consider the isotropic model for simplicity of exposition.

[11] G. B. Arfken and H. J. Weber, *Mathematical Methods for Physicists*, 4th ed. (Academic Press, New York, 1995).

[12] G. Kofman, G. Kurizki, and B. Sherman, J. Mod. Opt. **41**, 353 (1994).

[13] P. W. Milonni, *Fast Light, Slow Light and Left-Handed Light* (Taylor & Francis, New York, 2005).

[14] S. E. Harris, J. E. Field, and A. Kasapi, Phys. Rev. A **46**, R29 (1992).

[15] The coupling constant in Eq. (A6) results from using the $\vec{A}\cdot\vec{p}$ form of the atom-field interaction. In the $-\vec{E}\cdot\vec{r}$ form of the interaction, the atom-field coupling constant is given by $C_{\vec{k}\lambda nm}=\frac{1}{\hbar}\left(\frac{2\pi\hbar\omega_{\vec{k}}}{V}\right)^{1/2}\vec{\mu}_{nm}\cdot\vec{e}_{\vec{k}\lambda}$, independent of ω_{mn}.

[16] S. K. Lyo and D. H. Huang, Phys. Rev. B **64**, 115320 (2001).